September 2004 • NREL/SR-500-35061

Subcontractor Report

Wind Turbine Field Testing of State-Space Control Designs

August 25, 2003–November 30, 2003

K.A. Stol
University of Auckland
Auckland, New Zealand

L.J. Fingersh
National Renewable Energy Laboratory
Golden, Colorado

National Renewable Energy Laboratory
1617 Cole Boulevard, Golden, Colorado 80401-3393
303-275-3000 • www.nrel.gov

Operated for the U.S. Department of Energy
Office of Energy Efficiency and Renewable Energy
by Midwest Research Institute • Battelle

Contract No. DE-AC36-99-GO10337

September 2004 • NREL/SR-500-35061

Wind Turbine Field Testing of State-Space Control Designs

August 25, 2003–November 30, 2003

K.A. Stol
University of Auckland
Auckland, New Zealand

L.J. Fingersh
National Renewable Energy Laboratory
Golden, Colorado

NREL Technical Monitor: A. Wright

Prepared under Subcontract No. AAM-3-33231-01

National Renewable Energy Laboratory
1617 Cole Boulevard, Golden, Colorado 80401-3393
303-275-3000 • www.nrel.gov

Operated for the U.S. Department of Energy
Office of Energy Efficiency and Renewable Energy
by Midwest Research Institute • Battelle

Contract No. DE-AC36-99-GO10337

Available electronically at http://www.osti.gov/bridge

Available for a processing fee to U.S. Department of Energy and its contractors, in paper, from:

U.S. Department of Energy
Office of Scientific and Technical Information
P.O. Box 62
Oak Ridge, TN 37831-0062
phone: 865.576.8401
fax: 865.576.5728
email: mailto:reports@adonis.osti.gov

Available for sale to the public, in paper, from:

U.S. Department of Commerce
National Technical Information Service
5285 Port Royal Road
Springfield, VA 22161
phone: 800.553.6847
fax: 703.605.6900
email: orders@ntis.fedworld.gov
online ordering: http://www.ntis.gov/ordering.htm

This publication received minimal editorial review at NREL

Printed on paper containing at least 50% wastepaper, including 20% postconsumer waste

WIND TURBINE FIELD TESTING OF STATE-SPACE CONTROL DESIGNS

Karl A. Stol
Lee J. Fingersh

ABSTRACT

This report investigates the application of advanced pitch control algorithms on a 600-kW variable-speed, variable-pitch wind turbine known as the Controls Advanced Research Turbine (CART). A design approach is outlined to test both time-invariant and periodic control methods for fatigue load reduction over all operating wind speeds. Practical implementation issues are identified and addressed. Test data and preliminary performance comparisons are presented to support the approach.

Contents

List of Tables

List of Figures

NOMENCLATURE

A	Plant model state matrix
B	Plant model control input matrix
B_d	Plant model disturbance input matrix
C	Plant model output matrix
F	Disturbance model state matrix
G	Full-state feedback gain
I	Identity matrix
J	Quadratic cost scalar for regulator design
J_E	Quadratic cost scalar for estimator design
$\overline{K}$	State estimator gain
L	State estimator matrix
M	State estimator input matrix
$\underline{M}_{bflap}$	Vector of blade root flapwise bending moments
M_{tfa}	Tower fore-aft base bending moment
M_{tss}	Tower side-to-side base bending moment
N_b	Number of blades
P	Augmented feedback gain matrix
P_{rated}	Rated power
Q	State weighting matrix for optimal control
Q^E	State estimate weighting matrix for optimal control
R	Input weighting matrix for optimal control
R^E	Measurement weighting matrix for optimal control
T	Fundamental period of model dynamics
T_g	Generator torque
T_s	Discrete-time sampling period
$\underline{q}$	Vector of SymDyn DOFs
r	Rotor radius
s	Laplace operator
t	Time
$\underline{u}$	Plant model control input vector
u_d	Disturbance input
w	Horizontal wind speed at hub-height
$\underline{x}$	Plant model state vector
$\underline{y}$	Plant model measured output vector
$\underline{z}$	Augmented plant state vector
$\underline{z}_d$	Disturbance state vector
Φ	State transition matrix
Θ	Disturbance model output matrix
β_1, β_2	Blade #1 and #2 flap angle DOFs in SymDyn
ε	Shaft compliance (twist) angle DOF in SymDyn
ρ	Air density
τ_1	Tower fore-aft angle DOF in SymDyn
τ_2	Tower side-to-side angle DOF in SymDyn
ϕ	Hub teeter angle DOF in SymDyn
λ	Tip-speed ratio

θ_{com} Commanded blade pitch angle
$\underline{\theta}$ Vector of full-span blade pitch angles
$\int \Delta\theta$ Integrated pitch error state
ω Rotor speed ($=\dot{\psi}$ in SymDyn)
ω_{rated} Rated rotor speed
ψ , $\dot{\psi}$ Rotor azimuth angle DOF and speed in SymDyn

dots above symbols represent time derivatives, e.g., $\dot{\psi}$.

hats above symbols represent estimated quantities, e.g., $\hat{\underline{z}}$.

bars above symbols represent augmented estimator system matrices, e.g., $\overline{K}$
bars below symbols represent a vector quantity, e.g., $\underline{q}$.

'T' superscript of a matrix or vector represents transposition.
'op' subscript represents an operating point quantity.
'm' subscript represents the SymDyn model.
'a' subscript represents the pitch actuator model.
'disc' subscript represents the discrete-time equivalent controller.
'k' subscript represents a vector index for the discrete-time equivalent controller.
Δ prefix represents a perturbation from the operating point.

1. INTRODUCTION

State-space or modern control is a model-based approach, whereby an analytical model of a system is used internally by the control algorithm. The controller uses the model to estimate the current dynamics of the system, by updating state variables from known measurements, and then feeding back this information to calculate the control actions, e.g., pitch angles or rates. With state-space control, the design of feedback gains is a systematic process regardless of the number of sensors or available actuators.

Many studies of state-space pitch control for wind turbines have been performed using computer simulations to evaluate performance [1-6]. In [5,6], the author showed the potential for individual blade pitch control (IBC) to reduce blade fatigue equivalent loads by 13% without a significant effect on power capture. Practically, this means that blades could be designed lighter, larger, or with a longer lifetime – directly reducing the cost of energy. In order to realize these advantages it is important to test advanced control designs on an actual wind turbine to address the physical limitations. Field testing of controls provides validation of performance benefits and gives credibility to new designs. Testing also brings to light the many implementation issues that must be addressed for the benefit of future control objectives.

The Controls Advanced Research Turbine (CART) is a Westinghouse WTG-600, rated at 600 kW, located at the National Wind Technology Center in Colorado (Figure 1). It is an upwind machine with a nacelle tilt of 3.8°. The two-bladed teetering rotor has zero precone and a diameter of 43.3 m. Hub height is 36.6 m. Generator speed is rated at 1800 rpm. Through a two-state gearbox with a reduction ratio of 43.165, the rated rotor speed is ω_{rated} = 41.7 rpm. Potential control actuators include individual blade pitch angle by electromechanical servos and generator torque command via power electronics through an induction generator. A yaw drive is also present but, because of a yaw rate limit of 0.5°/s, its sole function is to track wind direction changes. The turbine is well instrumented with position encoders, strain gauges, accelerometers and anemometers, which contribute to 88 data channels recording at 100 Hz. The CART was commissioned in 2002 [7] and has been tested with both baseline and more advanced control algorithms [8]. The baseline controller performance is a basis for comparison in this paper.

Figure 1: The CART at the National Wind Technology Center

Variable-speed turbine operation can be divided into three regions (Figure 2). Region 1 describes start-up when wind speeds are below cut-in. Region 2 is between cut-in and rated wind speeds, just before the turbine generates rated power. A main objective of a controller in this region is to capture the maximum amount of energy from the wind. This is achieved by keeping blade pitch approximately constant and using generator torque to vary the rotor speed. With small pitch changes about the optimal angle, a controller can also reduce dynamic loads in the structure. In Region 3, between rated and cut-out wind speeds, wind power must be shed by the rotor to limit output power to the rated value. This is usually accomplished by keeping generator torque constant and commanding blade pitch angles. Structural fatigue loads can also be reduced in Region 3 via pitch commands. The overall goal of the control system is to meet different performance objectives in each operating region and make the transition between Regions 2 and 3 smoothly to avoid load spikes. For the CART, the cut-in wind speed is 5 m/s, the rated wind speed is approximately 12 m/s, and the cut-out wind speed is approximately 26 m/s.

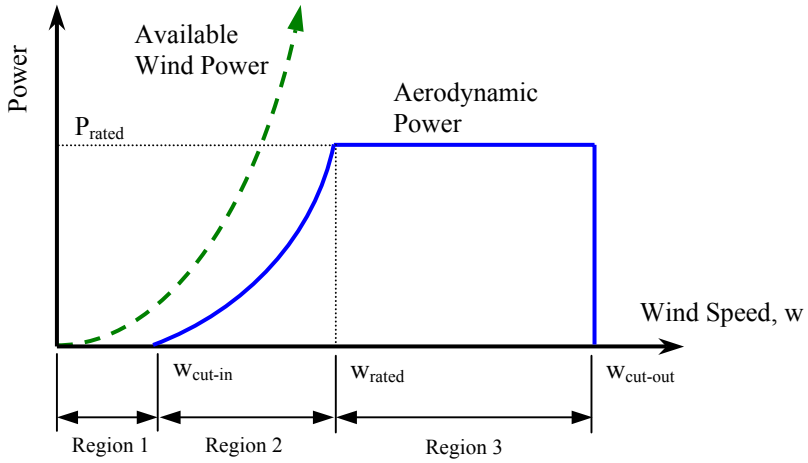

Figure 2: Idealized power curve to illustrate the operating regions of a variable-speed wind turbine

We begin by describing the different models of the CART, used in analytical form for state-space control or for simulation purposes. The following sections describe how the controllers are designed and implemented, and present sample test results.

2. CART MODELS

2.1 Turbine Properties

Properties for the CART are obtained from a variety of sources. Geometry and structural properties for the major components are detailed in [9]. These properties have been derived by systematic model tuning to a modal survey with the rotor parked, as well as from field data. Table 1 lists the first five modes from experiment results compared with an ADAMS® model constructed from the tuned data.

Table 1: Modal properties of the CART with the rotor parked and blades vertical

Mode No.	Modeshape Description	Exper. Results (Hz)	ADAMS Model (Hz)
1	1st tower fore-aft bending	0.86	0.87
2	1st tower lateral bending	0.88	0.86
3	1st shaft torsion	1.38	1.38
4	1st blade flap asymmetric	1.58	1.58
5	1st blade flap symmetric	2.06	2.06

Airfoil properties are taken from an earlier CART model in ADAMS and have not been tuned to match operational data.

Individual servo motors pitch each blade based on *rate* (not angle) commands from the CART control software. Separate hardware controllers convert these pitch rate signals into pitch torque commands and, at a lower level, motor current. The overall actuator rate response is very fast and, therefore, instead of modeling each pitch controller element, it is convenient to represent the closed-loop dynamics by the following first-order transfer function:

$$\frac{\dot{\theta}_{com}(s)}{\dot{\theta}(s)} = \frac{60.0}{s + 60.0} \quad . \tag{1}$$

Put simply, this expression represents a time lag between commanded pitch rates and actual pitch rates. The time constant of 1/60.0 = 0.017 seconds was found by least-squares fitting to field test data, as described in Appendix A.

2.2 SymDyn Model

SymDyn models of the CART are used to extract linear state-space representations, for control design, and for preliminary simulation testing.

SymDyn is a publicly available code [10] developed primarily for wind turbine controls research. SymDyn models the flexibility of the tower, drive train and blades as rigid bodies connected with torsional joint springs. A total of $8+N_b$ degrees of freedom (DOFs) are allowable, where N_b is the number of blades. The DOFs are all relative angular displacements measured between adjacent rigid components. The current version of SymDyn is written in Fortran and interfaced with MATLAB®. SymDyn calculates aerodynamic loads using a MATLAB interface to AeroDyn [11] subroutines, currently version 12.52. Wind inflow can either be provided by MATLAB variables or read from a file.

For the SymDyn CART models, we have chosen to use up to 7 DOFs, as illustrated in Figure 3 and listed below. The azimuth position DOF, ψ, measures the rotation of the drive shaft at the generator end in the low-speed shaft reference frame. Blade #1 is in the twelve o'clock position when $\psi = 0^o$ and $\varepsilon = 0^o$.

τ_1 Tower fore-aft deflection
τ_2 Tower side-to-side deflection
ψ Azimuth position
ε Shaft torsional deflection
φ Hub teeter
β_1 Blade #1 flap angle
β_2 Blade #2 flap angle

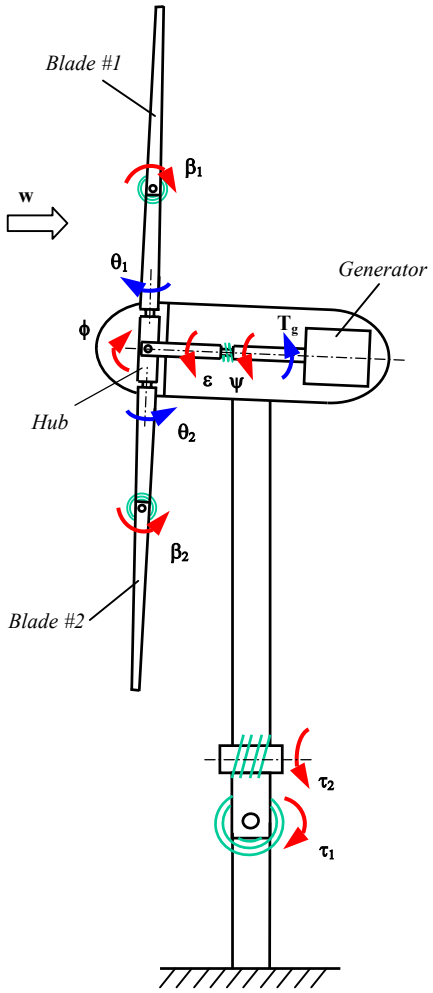

Figure 3: SymDyn DOFs and control inputs for CART modeling

Three control inputs are available. These are presented in Figure 3 and listed below. Generator torque signals are represented in the low-speed-shaft frame. That is, actual generator torque is 43.165 times greater, where the multiplier is the CART gearbox gear ratio. Blade pitch angles rotate the blade flap hinges such that flapwise bending is not purely out-of-plane motion.

T_g Generator torque
θ_1 Blade #1 pitch angle
θ_2 Blade #2 pitch angle

2.3 ADAMS Model

ADAMS is a commercial code that is capable of modeling the dynamics of flexible components with high fidelity. A current limitation in ADAMS is that systems can only be linearized when stationary. An ADAMS model of the CART is used for advanced simulation testing of control algorithms and, as we've already seen, for modal comparisons in tuning properties.

The ADAMS model contains 193 DOFs to represent fully flexible tower, drive-train, and blade components. The yaw DOF is locked. Aerodynamic loads are calculated using the same AeroDyn subroutines that are interfaced with SymDyn. Wind inflow must be read from a file.

3. BASELINE CONTROLLER

A classical control algorithm has been designed and implemented on the CART by Lee Fingersh [8]. Many hours of data have been collected using this algorithm with wind speeds spanning the full operating range of the turbine. These data provide a baseline with which to compare new control schemes.

The baseline controller comprises independent torque and collective pitch algorithms. Generator torque commands are calculated from a piecewise function, as illustrated in Figure 4. Fast power electronics and shaft torque feedback ensure the commands are achieved. The quadratic component, which is active during most of Region 2, is designed to keep the tip-speed ratio ($\lambda = \omega.r / w$) at the optimal value for maximum power at a given wind speed. Above 99% of the rated rotor speed ($\omega_{rated} = 41.7$ rpm), torque commands are constant at 3524 Nm. Between approximately 98% and 99% of ω_{rated}, the transition is linear, equivalent to a slip of 5%. A tower resonance avoidance scheme is active when the rotor speed approaches 26 rpm. At this speed twice-per-revolution vibration would excite the first tower bending modes. The resonance avoidance scheme uses a hysteresis loop to modify the generator torque command, so that the turbine spends less time around the critical speed. The scheme is effective in reducing tower vibration but theoretically must make a small sacrifice in energy capture, since the tip-speed ratio will stray from optimal.

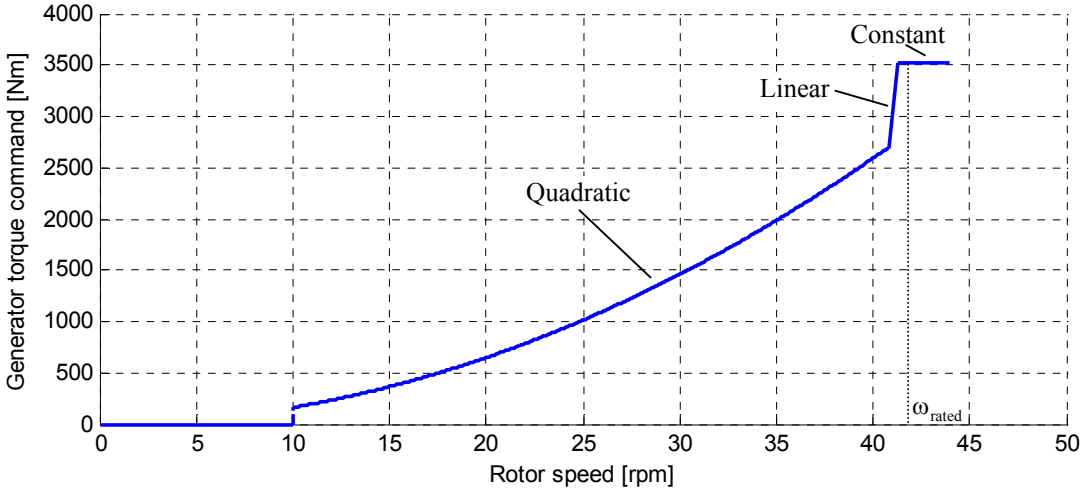

Figure 4: Generator torque profile for the baseline control algorithm

The pitch component of the baseline controller is a modified proportional-integral design. Conventional proportional and integral gains on rotor speed error have values of 40 deg.s/rad and 15 deg/rad respectively. Another term is added to calculate collective pitch commands based on the integral of rotor acceleration. This 'integrated-derivative' term has a gain of 30 deg/rad and serves to prevent rotor speed overshoot during the transition from Region 2 to Region 3. After the first time step in Region 3, this term has exactly the same effect as a proportional speed error

term. The pitch controller is active at all times in the algorithm. However, pitch commands have a lower saturation limit, determined by the profile illustrated in Figure 5. Above a tip-speed ratio of 6.0, the saturation limit is -1.0 deg, which is the optimal pitch angle for maximum aerodynamic power in Region 2.

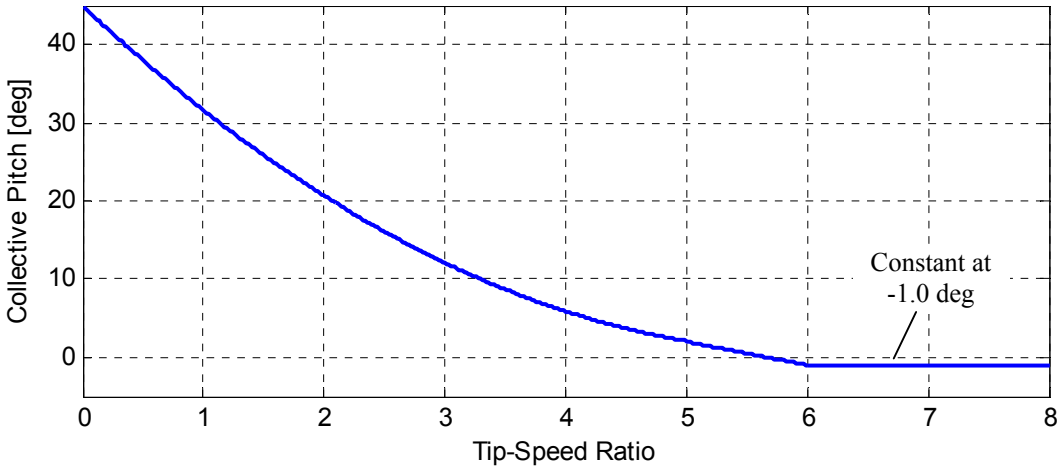

Figure 5: Pitch profile used as a saturation limit

Pitch angle commands are converted to pitch rate commands using

$$\dot{\theta}_{com} = 5.0(\theta_{com} - \theta) \ , \tag{2}$$

where θ is the measured pitch angle for a particular blade. This expression acts as a first-order filter, smoothing out high-frequency pitch command signals, measured pitch quantization, and sensor noise. In fact, the low gain of 5.0 was chosen so that drive train torsional vibration entering into the rotor speed signal would not cause pitch commands at the same frequency and subsequent drive train excitation.

4. LINEAR STATE-SPACE CONTROL

4.1 Linear Models

Linearization of the SymDyn CART model provides us with state-space representations for control system design. A linearization point is chosen within both Regions 2 and 3 based on operating conditions. The chosen points are defined in Table 2 and illustrated in Figure 6.

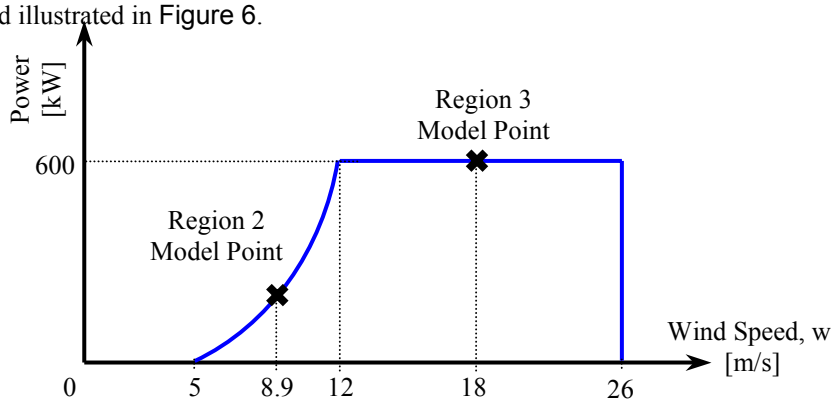

Figure 6: Linearization point locations on the approximate CART power curve

Table 2: Linearization point descriptions. *Generator torque is represented in the low-speed shaft reference frame.

	Region 2	Region 3
Hub-height wind speed, w_{op}	8.9 m/s	18.0 m/s
Mean rotor speed, ω_{op}	30.0 rpm	41.7 rpm
Generator torque*, T_{g_op}	61.6 kNm	152.1 kNm
Blade pitch, $\underline{\theta}_{op}$	-1.0 deg	10.8 deg

The inflow is steady with a vertical shear exponent of 0.2. Because of the sheared wind and the asymmetric nature of a two-bladed rotor, the turbine motion at the linearization points is periodic in time, with a period equal to $T = 2\pi/\omega_{op}$. This motion ($\underline{q}_{op}(t)$, $\dot{\underline{q}}_{op}(t)$, and $\ddot{\underline{q}}_{op}(t)$) is found by simulation of the nonlinear SymDyn model until a steady-state solution is reached. The linearization points also serve as set points or operating targets for the controllers. The Region 2 linearization point is chosen at a rotor speed greater than 26 rpm, where tower resonance will occur. Also, the operating wind speed is consistent with the optimal tip-speed ratio of 7.5, which is necessary to obtain maximum power in variable speed.

Linearized SymDyn models are represented by

$$\begin{cases} \dot{\underline{x}}_m = A_m \underline{x}_m + B_m \underline{u}_m + B_{d\_m} u_d \\ \underline{y}_m = C_m \underline{x}_m \end{cases}, \tag{3}$$

where

$$\underline{x}_m = \begin{bmatrix} \Delta\underline{q} \\ \Delta\dot{\underline{q}} \end{bmatrix}, \ \underline{u}_m = \begin{bmatrix} \Delta T_g \\ \Delta\underline{\theta} \end{bmatrix}, \ u_d = \Delta w \text{, and } \underline{y}_m \text{ are the desired measurements.}$$

The state, input, and output vectors contain components that are perturbations from the linearization point, hence, the use of the Δ symbol. The hub-height wind speed variation Δw is the only assumed disturbance to the model. The state-space matrices (A_m, B_m, B_{d_m}, and C_m) are time-periodic in general, with period T. A linear time-invariant (LTI) representation is constructed by averaging the matrices over one period.

Our pitch actuator model, Eq. (1), is already linear in terms of absolute pitch rate. Therefore, the model is also linear in terms of pitch rate perturbations. The equivalent state-space representation for the actuator model has four states, two for each blade:

$$\begin{cases} \dot{\underline{x}}_a = A_a \underline{x}_a + B_a \underline{u}_a \\ \underline{y}_a = C_a \underline{x}_a \end{cases}, \tag{4}$$

where

$$\underline{x}_a = \begin{bmatrix} \Delta\underline{\theta} \\ \Delta\dot{\underline{\theta}} \end{bmatrix}, \ \underline{u}_a = \dot{\underline{\theta}}_{com}, \ \underline{y}_a = \Delta\underline{\theta},$$

$$A_a = \begin{bmatrix} 0 & 0 & 1 & 0 \\ 0 & 0 & 0 & 1 \\ 0 & 0 & -60 & 0 \\ 0 & 0 & 0 & -60 \end{bmatrix},\ B_a = \begin{bmatrix} 0 & 0 \\ 0 & 0 \\ 60 & 0 \\ 0 & 60 \end{bmatrix}, \text{ and } C_a = \begin{bmatrix} 1 & 0 & 0 & 0 \\ 0 & 1 & 0 & 0 \end{bmatrix}.$$

When a collective pitch actuator is assumed, the state-space representation has only two states. For a Region 2 controller the actuator model is augmented by extra states to represent integrated pitch error. This special model will be described in Section 5.

Partitioning B_m into $B_m = \lfloor B_{Tg} \quad B_\theta \rfloor$ and combining (3) with (4), the result is a governing set of linear equations for SymDyn and the pitch actuators, referred to as the linear plant model:

$$\begin{cases} \dot{\underline{x}} = A\,\underline{x} + B\,\underline{u} + B_d\,u_d \\ \underline{y} = C\,\underline{x} \end{cases}, \tag{5}$$

where

$$\underline{x} = \begin{bmatrix} \underline{x}_m \\ \underline{x}_a \end{bmatrix},\ \underline{u} = \begin{bmatrix} \Delta T_g \\ \Delta\dot{\underline{\theta}}_{com} \end{bmatrix},\ u_d = \Delta w,\ \underline{y} = \begin{bmatrix} \underline{y}_m \\ \underline{y}_a \end{bmatrix},$$

$$A = \begin{bmatrix} A_m & B_\theta C_a \\ 0 & A_a \end{bmatrix},\ B = \begin{bmatrix} B_{Tg} & 0 \\ 0 & B_a \end{bmatrix},\ B_d = \begin{bmatrix} B_{d\_m} \\ 0 \end{bmatrix}, \text{ and } C = \begin{bmatrix} C_m & 0 \\ 0 & C_a \end{bmatrix}.$$

4.2 Gain Calculation Method

There are two components of the control system design: the calculation of full-state feedback gains and the calculation of estimator gains. When all the plant states $\underline{x}$ are known, as in the case when SymDyn is the designated simulation model, then the control inputs $\underline{u}$ are formed by

$$\underline{u} = G(t)\,\underline{x}, \tag{6}$$

which is referred to as full-state feedback (FSFB). An illustration of this is shown in Figure 7(a). When some or all the plant states are not known, as is the usual reality, then we may estimate the states online by supplying plant measurements $\underline{y}$. State estimation is achieved by incorporating the linear plant model (5) within the controller and using a gain $\overline{K}$ to determine how fast the estimator operates. Fast estimators amplify measurement noise, which forces us to compromise performance. When an estimator is combined with FSFB, where estimated instead of actual states are fed back, this is called a *realizable* controller. An illustration is shown in Figure 7(b).

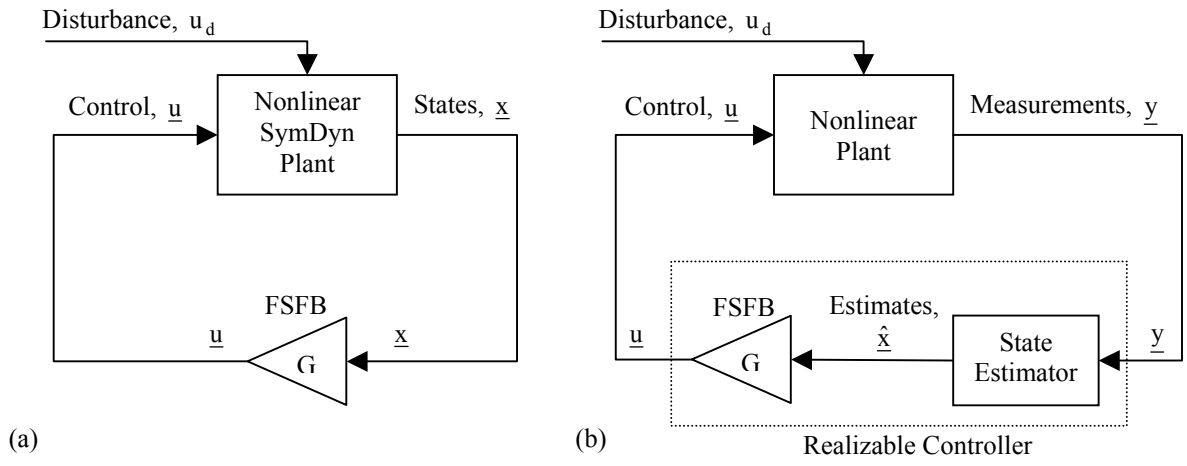

Figure 7: Controllers in operation: (a) full-state feedback control, (b) realizable control

The full-state gains G are designed for desirable transient behavior using optimal control techniques [12]. For linear systems, this is known as linear quadratic regulation (LQR). With LQR, we seek G to minimize the quadratic cost function

$$J = \int_0^\infty \left(\underline{x}(t)^T Q \, \underline{x}(t) + \underline{u}(t)^T R \, \underline{u}(t) \right) dt \,, \tag{7}$$

subject to the dynamics of the plant (5), and the chosen weightings on state regulation, Q, and control usage, R. Fast state regulation and low actuator usage are competing objectives and, therefore, the Q and R weightings allow us to trade off different performance objectives with actuator bandwidth. For control of the CART, R is always set to the identity matrix, and diagonal entries of Q are varied to achieve desired state regulation performance. Choice of Q will be further discussed in Section 6. With A, B, Q, and R we can calculate a unique G. For the time-invariant (LTI) case, there are built-in MATLAB functions to perform this calculation. When a periodic controller is desired, user-written functions are required to perform this task [5].

The next stage of controller design involves the calculation of estimator gains. We first augment the linear plant model to include a disturbance waveform generator. This will allow us to estimate the disturbance input, hub-height wind speed, without measuring it directly. While not utilized in the present CART controllers, an estimate of wind speed could be valuable in future algorithms. We also observed in simulation that regulation performance is improved in comparison to that of estimators without disturbance augmentation. From Disturbance Accommodating Control theory [13], the disturbance waveform is described by an ordinary differential equation:

$$\begin{cases} \dot{\underline{z}}_d = F \, \underline{z}_d \\ u_d = \Theta \, \underline{z}_d \end{cases} . \tag{8}$$

To generate rapidly changing wind speeds, a step waveform is chosen, requiring $F = 0$ and $\Theta = 1$ (so $\dot{z}_d = 0$ and $u_d = z_d = \Delta w$). Defining an augmented state vector as

$$\underline{z} \equiv \begin{bmatrix} \underline{x} \\ z_d \end{bmatrix} = \begin{bmatrix} \Delta \underline{q} \\ \Delta \dot{\underline{q}} \\ \Delta \underline{\theta} \\ \Delta \dot{\underline{\theta}} \\ \Delta w \end{bmatrix} , \tag{9}$$

and combining (5) and (8), the augmented linear plant model is described by

$$\begin{cases} \dot{\underline{z}} = \overline{A}\,\underline{z} + \overline{B}\,\underline{u} \\ \underline{y} = \overline{C}\,\underline{z} \end{cases}, \tag{10}$$

where

$$\overline{A} = \begin{bmatrix} A & B_d \\ 0 & 0 \end{bmatrix},\ \overline{B} = \begin{bmatrix} B \\ 0 \end{bmatrix},\ \text{and}\ \overline{C} = \begin{bmatrix} C & 0 \end{bmatrix}.$$

Following standard state-estimator theory, we use the available state information from the measured output $\underline{y}$ to reconstruct all states. This is achieved by

$$\begin{cases} \dot{\hat{\underline{z}}} = \overline{A}\,\hat{\underline{z}} + \overline{B}\,\underline{u} + \overline{K}(\underline{y} - \hat{\underline{y}}) \\ \hat{\underline{y}} = \overline{C}\,\hat{\underline{z}} \end{cases}, \tag{11}$$

where $\overline{K}$ are the estimator gains. To calculate $\overline{K}$, we use the property of duality and solve another LQR problem. Here, the quadratic cost function is

$$J_E = \int_0^\infty \left(\hat{\underline{z}}(t)^T Q^E\, \hat{\underline{z}}(t) + \underline{y}(t)^T R^E\, \underline{y}(t) \right) dt, \tag{12}$$

which has a similar form to (7). If system noise information is known, then the weightings Q^E and R^E can be chosen to equal terms in the plant output noise covariance matrix. This is a common technique for time-invariant systems, and the design is referred to as LQG (Linear Quadratic with Gaussian noise) [12]. However, for the CART estimator designs, we choose entries in the Q^E and R^E matrices based on observed performance during simulation. Generally, R^E is set to the identity matrix, and diagonal entries of Q^E are adjusted to achieve adequate estimator properties. Specific choices of Q^E and R^E will be detailed in Section 6. With $\overline{A}$, $\overline{C}$, Q^E and R^E we can now calculate a unique $\overline{K}$. As in the FSFB case, it is relatively straightforward to generate a time-invariant estimator using MATLAB functions, whereas a periodic estimator requires special attention [5].

Combining (6) and (11), the realizable controller is described by

$$\begin{cases} \dot{\hat{\underline{z}}} = L\,\hat{\underline{z}} + M\,\underline{v} \\ \underline{u} = P\,\hat{\underline{z}} \end{cases}, \tag{13}$$

where $\underline{v} = \begin{bmatrix} \underline{u} \\ \underline{y} \end{bmatrix}$, $L = \overline{A} - \overline{K}\,\overline{C}$, $M = \begin{bmatrix} \overline{B} & \overline{K} \end{bmatrix}$, and $P = \begin{bmatrix} G & 0 \end{bmatrix}$.

Recall that the control input vector $\underline{u}$ includes both torque and pitch rate commands. In the state-space control algorithms tested by the authors, torque commands are calculated by the same algorithm used in the baseline controller of the previous section. Only the pitch rate commands are generated by the method above. However, torque commands are retained in the estimator design to improve its performance.

4.3 Discrete-Time Equivalent Controllers

We have presented a state-space control methodology that assumes continuous-time operation. However, the CART control algorithm must run on a digital computer that refreshes all measurements and command signals at the rate of

100 Hz, i.e., with a sampling period of $T_s = 0.01$ sec. To operate in discrete-time, an equivalent control system is generated from the continuous-time version (13).

The general form of the discrete-time controller is

$$\begin{cases} \underline{u}_k = P_{disc}\, \hat{\underline{z}}_k \\ \hat{\underline{z}}_{k+1} = L_{disc}\, \hat{\underline{z}}_k + M_{disc}\, \underline{v}_k \end{cases}, \; k = 1, 2, 3, \ldots, \tag{14}$$

where the series $\hat{\underline{z}}_1$, $\hat{\underline{z}}_2$, $\hat{\underline{z}}_3$, etc., are the state estimate vectors for each time step, determined by some initial condition $\hat{\underline{z}}_0$ and the series of inputs $\underline{v}_1$, $\underline{v}_2$, $\underline{v}_3$, etc. The control input vector $\underline{u}_k$ (i.e., pitch rate commands) must be calculated first because it forms part of $\underline{v}_k$ and is subject to saturation.

For LTI control,

$L_{disc} = e^{L.T_s}$, a matrix exponential;
$M_{disc} = (L_{disc} - I).L^{-1}.M$, and
$P_{disc} = P$.

For periodic control,

$L_{disc}(t) = \Phi(t + T_s, t)$,
$\Phi(t,0)$ is the state transition matrix for L(t),
$M_{disc}(t) = \int_t^{t+T_s} \Phi(t + T_s, \tau).M(\tau).d\tau$, and
$P_{disc}(t) = P(t)$.

The system matrices $L_{disc}(t)$, $M_{disc}(t)$, and $P_{disc}(t)$ are time-continuous and periodic with period T. To implement, the period is discretized into 50 equal time steps, and the system matrices are formed into lookup tables. Low-speed shaft azimuth position and linear interpolation are then used to determine the values of the matrices at any particular time.

4.4 Choosing Controller Objectives and Variables

The ideal objective of a wind turbine control system would be to optimize power capture while reducing fatigue damage to critical components over all wind conditions. In the current implementation of state-space control, we focus on fatigue mitigation in Regions 2 and 3 independently while maintaining the same power capture as the baseline control design. To achieve this, we use blade pitch actuation and generate torque commands via the existing baseline algorithm. Even with this design simplification, we implement state-space control in stages so that we can readily identify and manage the many implementation issues.

Table 3 describes the stages of controller development as a matrix of test cases. Along the top of the matrix are different operating regions or objectives, beginning with simple speed regulation in Region 3 to match the main objective of the baseline PI algorithm. This is followed by simultaneous speed regulation and fatigue load mitigation in Region 3, then fatigue mitigation in Region 2. Along the side of the matrix are the two linear control methods investigated: time-invariant control coupled with collective pitch actuation and time-periodic control with individual pitch. The other two combinations of control methods (time-invariant with individual pitch and periodic with collective pitch) were not explored because of time constraints.

Table 3: Test case matrix

		Operating Region and Objective		
		Region 3 Speed Regulation	**Region 3 Speed Reg. and Fatigue Mitigation**	**Region 2 Fatigue Mitigation**
Control Method	**Time-Invariant Control, Collective Pitch**	Test Case ①	Test Case ②	Test Case ⑤
	Periodic Control, Individual Pitch	Test Case ③	Test Case ④	Test Case ⑥

The six test cases in Table 3 are numbered in order of realization, progressing from the simplest design to the more complex. The Region 2 controller designs (test cases 5 and 6) are implemented with Region 3 controllers as well (from test cases 2 and 4) to investigate region transition issues. Each test case is examined to determine the minimum number of SymDyn DOFs (and therefore controller states) that are needed to capture structural dynamics that are relevant to the specific objectives. For example, a suitable controller for Test Case 1 can be constructed using a single DOF, azimuth position, while Test Case 4 would need seven DOFs. CART measurements must then be chosen to adequately reconstruct the turbine's dynamics in the state estimator. Common to all successful designs is the use of azimuth position and pitch angle measurements. Specific sets of SymDyn DOFs and measurements will be described in Section 6.

4.5 Test Procedure and Tuning

Given a particular test case from Table 3, a suitable controller is designed and tested following the flow chart in Figure 8. The test process is designed to analyze a controller against different simulation plants with increasing complexity, thereby isolating potential problem sources and maximizing the productivity of field testing. At each stage in the process, control gains are tuned or algorithms are debugged. Turbulent wind input sent to each simulator is based on hub-height wind speeds within the desired operating region. With reference to Figure 8, each test stage is further described below.

1. Following the design of FSFB gains, they are tested directly on a nonlinear SymDyn model in MATLAB/Simulink® where all the system states are known. Regulation performance is assessed and gains are retuned (by modifying entries in Q) to account for nonlinear effects being introduced.

2. Once estimator gains have been designed, the control system arrays (P_{disc}, M_{disc}, and L_{disc}) are exported to text files (ctrlarr.dat, ctrlarr2.dat, or ctrlarr3.dat) and the control algorithm is coded in C to replicate the subroutines used on the CART. It is much simpler to debug source code after a short simulation run than after a field test. The full realizable controller is tested with a nonlinear SymDyn model to assess state estimation performance when only a limited set of plant measurements are available. Consequently, estimator and/or FSFB gains are tuned by modifying entries in Q^E, R^E, and Q.

3. Testing on an ADAMS model with flexible blades, drive train and tower components brings to light the possibility of exciting higher order modes that are not captured with SymDyn. Since ADAMS simulation runs take longer to complete it is fortunate that little or no gain tuning has been necessary at this stage. Also. it is not practical to interface the controller C code with ADAMS, so no further code debugging is made at this point.

4. The last stage before field testing is simulation with a simple CART model built into the CART software. This simulator integrates a single-state (rotor speed) and a lookup table for aerodynamic torque. Despite its dynamic simplicity, this simulator is effective in catching many C code implementation bugs and in highlighting region transition problem. It is also effective as an independent check of speed regulation performance. Since the simulator does not produce many of the measurement signals that the more

complex state-space controllers assume (such as bending loads), there are situations when the simulator predicts dynamic instability when the other simulator models or actual turbine do not.

5. Field testing usually involves continuous monitoring of the turbine's health to ensure that sensor difficulties do not adversely affect the controller's performance. There may also be residual bugs in the code that do not precipitate until the turbine is sequenced through initialization and startup procedures. In particular, run-time memory size is limited, which affects the number and size of arrays that can be allocated space. This limitation has affected the number of time steps that the periodic control arrays are discretized into (hence, the choice of 50 steps). In some circumstances it is necessary to fine tune some of the gains to deal with region transition problems.

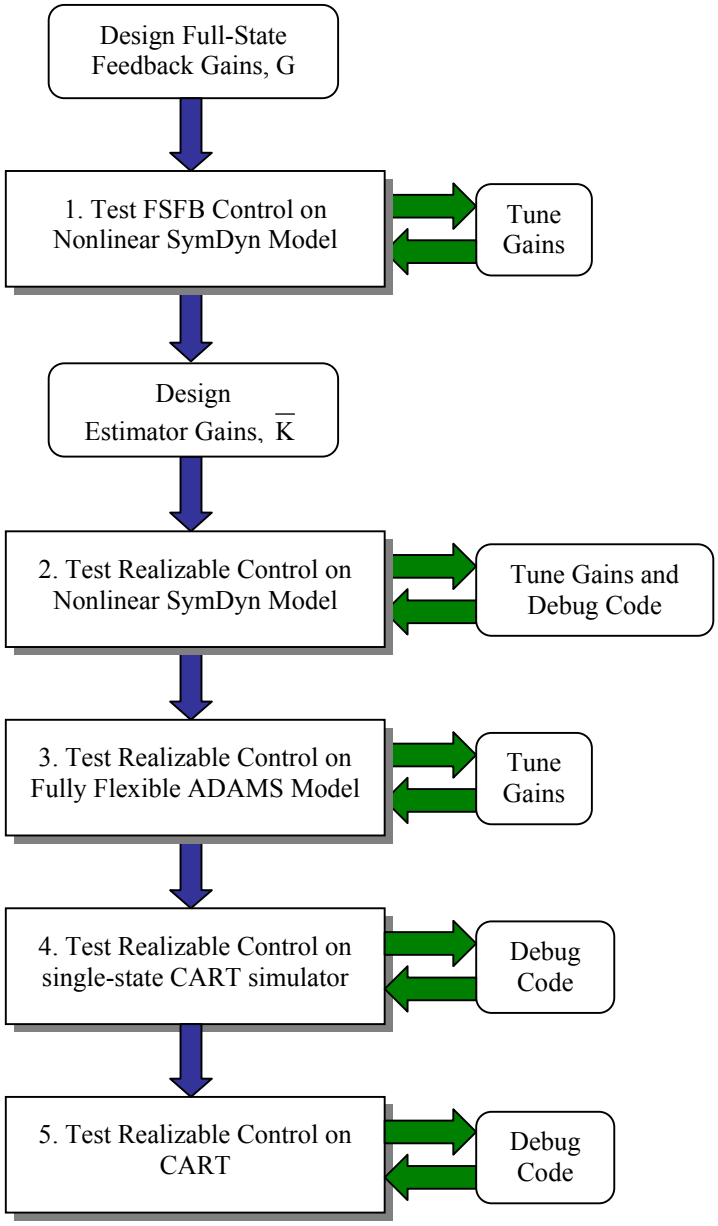

Figure 8: Control design testing process

To compare the performance of a state-space control design with the baseline controller, a number of different measures are calculated, as shown in Table 4. Root-mean-square (RMS) rotor speed error is used only in Region 3, while the mean shaft power measure is restricted to Region 2.

Table 4: Controller performance measures

Measure	Units
RMS rotor speed error	rpm
Mean shaft power	kW
Maximum pitch rate	deg/s
Maximum pitch acceleration	deg/s^2
RMS pitch acceleration	deg/s^2
Tower base fore-aft moment fatigue damage equivalent load (DEL)	kNm
Tower base side-to-side moment fatigue DEL	kNm
Low-speed-shaft torque fatigue DEL	kNm
Blade-root flap moment fatigue DEL	kNm

Pitch rate acceleration metrics quantify actuator usage and allow us to check whether a controller will perform within the CART's physical limitations. The maximum pitch rate allowed is 18 deg/s and is coded as a saturation limit. Electrical current limits for the pitch servos are 60 amps maximum and 35 amps RMS. Assuming there are no friction losses, these currents correspond to a maximum pitch acceleration of 155 deg/s^2 and maximum RMS pitch acceleration of 90 deg/s^2. To be conservative, controller performance is checked to ensure pitch that accelerations are less than 150 deg/s^2 maximum and 70 deg/s^2 RMS.

Fatigue damage equivalent loads (DELs) are calculated using rainflow counting [14], Miner's linear damage rule [15], and a reference frequency of 1.0 Hz. Tower bending moments are measured at 9.3 m up from the ground to correspond to strain gauge locations. Fore-aft and side-to-side tower moments are calculated by resolving the strain gauge measurements based on nacelle yaw position.

MATLAB and Simulink by The Mathworks, Inc., are used throughout the controller development process, via user-written scripts code, functions and simulation block diagrams. Beginning with CART properties prepared in a general format, SymDyn nonlinear models and ADAMS datasets are prepared automatically. SymDyn is linearized, control gains are generated, and control matrices are exported to text files, all using MATLAB script code. All simulations with SymDyn are performed in Simulink; then, all processing and graphing of results are performed in MATLAB. Having a single computational environment to work in greatly reduces the time required for controller development and increases the feasible number of design iterations.

5. IMPLEMENTATION ISSUES

5.1 Steady-State Speed Error in Region 3

An objective of a Region 3 controller is to regulate rotor speed to the rated value during wind inflow variations. Our controller has a state for rotor speed error $\Delta\dot{\psi}$ so it obvious that we should weight this state in the LQR scheme, resulting in a proportional feedback gain. If this design is then simulated using a staircase of wind speeds, the result is steady-state errors in rotor speed, as shown by the solid line in Figure 9. The errors are greatest when the wind speed is furthest from the linearization point speed w_{op}. During stochastic winds, rotor speed errors result mainly from transient behavior, and steady-state errors are masked. However, overspeed conditions are more likely to occur; therefore, this design is unsuitable. Steady-state errors are removed by including feedback that is proportional to the integral of rotor speed error, as in PI control. In state-space control this is achieved by specifying an LQR weighting on the azimuth error state $\Delta\psi$, which is the integral of rotor speed error by definition. The dashed line in Figure 9 illustrates the effectiveness of this approach.

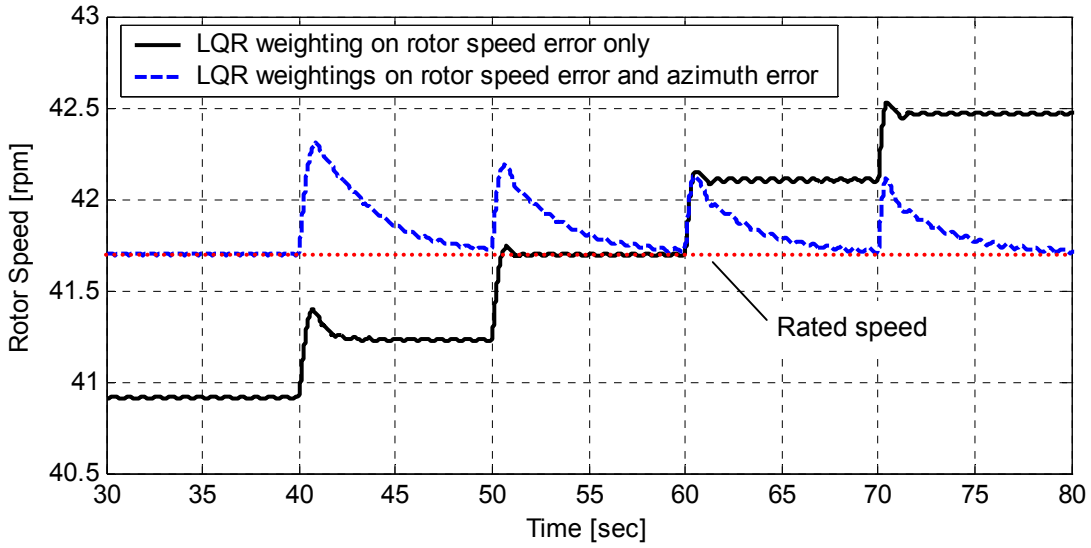

Figure 9: Results from an example state-space control design given a staircase of wind speeds

5.2 Pitch Angle Saturation

In many situations it is necessary to include a pitch angle saturation limit. Imposing such a limit with the baseline PI controller is simple, because the design is providing pitch angle commands. The state space controllers command pitch rate; therefore, there is no direct method for angle saturation. To perform this task, pitch command signals are generated using

$$\theta_{com} = \frac{\dot{\theta}_{com}}{5.0} + \theta \tag{15}$$

for each blade. Following angle saturation, pitch rate commands are then reconstructed using

$$\dot{\theta}_{com} = 5.0\left(\theta_{com} - \theta\right), \tag{16}$$

the same relationship used in the baseline PI algorithm, Eq. (2).

5.3 Region Transition

In the implemented control algorithm, only one state-space control design is active at any particular time step. The current value of rotor speed is used to switch between the available designs. Above 95% of rated speed (i.e., 39.6 rpm), the Region 3 design is active. This critical speed is chosen to give the controller enough time to react to high accelerations caused by sudden wind speed increases. When a Region 2 control design is also coded, it is active between 20.0 rpm and 39.6 rpm. Below 20 rpm, we expect that the Region 2 controller would operate too far from its linearization point of 30.0 rpm to be effective in reducing fatigue loads.

When the implemented algorithm contains only a Region 3 controller, e.g., in test cases 1 and 2, the state estimates $\hat{\underline{z}}$ are initialized to predetermined values at the first time step in which the controller is active. Initializing the states to nonzero values helps to reduce the time it takes for estimator transients to die down, i.e., for state estimates to reflect the actual motion of the turbine. This is critical during Region 3 control startup, because the rotor may be accelerating quickly and overspeed will occur unless the controller generates appropriate pitch rate commands.

When the control algorithm contains both Region 2 and Region 3 designs, e.g., in test cases 5 and 6, the state estimates can be initialized by a different method. The Region 2 controller will become active at 20 rpm and, at this low speed, state estimates can be initialized to zeros without concern for estimator transients. As the turbine accelerates through 39.6, rpm the Region 2 controller state estimates can be used as initial conditions for the Region

3 controller (and vice-versa on speed deceleration). In contrast to supplying fixed initial conditions, handing off state estimates in this way provides continuity during speed changes and improves transition performance, in contrast to supplying fixed initial conditions. Generally, the Region 2 and 3 controllers will not have the same set of states, and only common states can be handed off. However, it is the common states that are the most important during transition, namely azimuth error $\Delta\psi$, rotor speed error $\Delta\dot{\psi}$, wind speed error Δw, and pitch actuator states: $\Delta\underline{\theta}$ and $\Delta\dot{\underline{\theta}}$. Recall that the states are defined as perturbations about a particular linearization point. Therefore, state estimates are adjusted to take into account the different linearization points used in the Region 2 and 3 designs.

If the Region 3 controller is active and the rotor speed is below rated, commanded pitch rates will generally be negative to accelerate the rotor. At low wind speeds, the situation then exists where pitch angles are approaching the optimal value of -1.0 deg and commanded pitch rates are still negative. At this point, pitch angle saturation is necessary, following the procedure described in Section 5.2, to ensure that the blades do not stall. If the rotor speed remains above 39.6 rpm and the pitch angles are saturated, an undesirable control condition called wind-up can occur. If wind occurs, azimuth error will become negative and continue to decrease without bounds. Not until the rotor speed is greater than rated will the azimuth error increase. Meanwhile, pitch angles will remain saturated, leading to the likelihood of overspeed. To prevent wind-up, we saturate azimuth error at -20.0 deg, which works well in practice but is not the best solution. Perhaps a better method would be to make the transition to the Region 2 controller immediately, thus incorporating a more complex trigger mechanism not solely dependent on rotor speed.

5.4 Steady-State Pitch Error in Region 2

The Region 2 state-space controller is developed to reduce fatigue loads using only small pitch changes. The foundation of the design is to keep pitch angles within ±1.0 deg of the linearization point and optimal angle of -1.0 deg. Just as nonlinearities in aerodynamics cause steady-state speed errors in Region 3, they also cause steady-state pitch errors in Region 2. To eliminate these pitch errors, the CART pitch actuator model (4) is augmented by integral pitch error states, resulting in

$$\underline{x}_a = \begin{bmatrix} \Delta\underline{\theta} \\ \Delta\dot{\underline{\theta}} \\ \int \Delta\underline{\theta} \end{bmatrix}, \quad \underline{u}_a = \dot{\underline{\theta}}_{com}, \quad \underline{y}_a = \Delta\underline{\theta}, \tag{17}$$

$$A_a = \begin{bmatrix} 0 & 0 & 0 & 0 & 1 & 0 \\ 0 & 0 & 0 & 0 & 0 & 1 \\ 0 & 0 & 0 & 0 & -60 & 0 \\ 0 & 0 & 0 & 0 & 0 & -60 \\ 1 & 0 & 0 & 0 & 0 & 0 \\ 0 & 1 & 0 & 0 & 0 & 0 \end{bmatrix}, \quad B_a = \begin{bmatrix} 0 & 0 \\ 0 & 0 \\ 60 & 0 \\ 0 & 60 \\ 0 & 0 \\ 0 & 0 \end{bmatrix}, \text{ and } C_a = \begin{bmatrix} 1 & 0 & 0 & 0 & 0 & 0 \\ 0 & 1 & 0 & 0 & 0 & 0 \end{bmatrix}.$$

The combined plant state vector is then defined by

$$\underline{z} = \begin{bmatrix} \Delta\underline{q} \\ \Delta\dot{\underline{q}} \\ \Delta\underline{\theta} \\ \Delta\dot{\underline{\theta}} \\ \int \Delta\underline{\theta} \\ \Delta w \end{bmatrix}. \tag{18}$$

In the full-state feedback LQR design, weightings on the $\int \Delta\underline{\theta}$ states provide the necessary integral feedback to remove pitch angle steady-state errors.

5.5 Incorporating a Pitch Profile in Region 2

To facilitate the comparison with the baseline controller, the pitch profile described in Section 3 (Figure 5) is incorporated into the state-space control algorithm. This scheme involves pitching the blades in Region 2 above the optimal -1.0 deg value when the tip-speed ratio is greater than 6.0. Since the state-space control design commands pitch rate, we cannot specify pitch angle directly. Also, since it desirable for the Region 2 controller to make small pitch changes above and below the nominal angle, we cannot employ the saturation method described in Section 5.2. Instead, the desired pitch angle determined by the pitch profile is used to modify the measured pitch angle signal, as follows.

Ordinarily, the controller uses measured pitch angles that are represented as perturbations about the linearization point, i.e.,

$$\Delta\theta = \theta_{\text{measured}} - \theta_{\text{op}} .$$

Recall that the linearization point for pitch angle in Region 2 is θ_{op} = -1.0 deg (from Table 2). The result is a controller that generates pitch rate commands so that the mean pitch angle is -1.0 deg. By using the pitch angle from the desired pitch profile (which is a function of tip-speed ratio, $\theta_{\text{des}}(\lambda)$), in place of θ_{op} in the pitch measurement calculation, i.e.,

$$\Delta\theta = \theta_{\text{measured}} - \theta_{\text{des}}(\lambda) ,$$

the controller now tracks to the desired pitch angle.

6. TEST RESULTS

Following the test procedure described in Section 4.3, test data were collected on the CART for all six test cases. A complete listing of the test data file names, together with controller variables and performance comments, is provided in Appendix B. A complete analysis of controller performance is beyond the scope of this report; however, a summary of results is given below.

6.1 Collected Data

A total of 158 10-minute data sets (3.2 gigabytes) were collected between January 2, 2003, and August 4, 2003. This amounts to 26.3 hours of data distributed between the test cases as shown in Table 5. Because the Region 2 control algorithms (in test cases 5 and 6) were always tested with Region 3 algorithms (in test cases 2 and 4, respectively), the test hours are included in both. Only three data sets were collected for test case 3 (0.5 hours), because this simple case was used only for code debugging and not for gain tuning purposes. Unfortunately, very little data were collected using the more advanced periodic, individual pitch controllers (test cases 4 and 6) because of the lack of suitable operating conditions and turbine maintenance problems. However, at the time of writing, plans were being made to collect supplementary data with these designs.

The controller variables constituting the final control design from each test case is summarized in Table 6. The LQR weightings used in each design can be found in Appendix B. The measurements listed in

Table **6** are expressed in a form consistent with the SymDyn-based design methodology, and in some cases, they represent a slightly different set of CART measurement channels. Table 7 is provided to explain the differences. In addition to the CART output channels listed, the periodic controllers use low-speed shaft position (channel 16) to synchronize the periodic arrays.

Table 5: Test case matrix with hours of data collected

		Operating Region and Objective		
		Region 3 Speed Regulation	**Region 3 Speed Reg. and Fatigue Mitigation**	**Region 2 Fatigue Mitigation**
Control Method	**Time-Invariant Control, Collective Pitch**	① *5.7 hours*	② *18.0 hours*	⑤ *13.0 hours*
	Periodic Control, Individual Pitch	③ *0.5 hours*	④ *2.2 hours*	⑥ *0.7 hours*

Table 6: Final controller variables for each test case

Test Case	Design	SymDyn DOFs	States	Measurements
①	R3 spd reg., TI coll. pitch	1 $\{\psi\}$	5 $\{\Delta q, \Delta\dot{q}, \Delta\theta, \Delta\dot{\theta}, \Delta w\}$	2 $\{\Delta\psi, \Delta\theta\}$
②	R3 TI coll. pitch	5 $\{\tau_1, \psi, \varepsilon, \beta_1, \beta_2\}$	13 $\{\Delta\underline{q}, \Delta\underline{\dot{q}}, \Delta\theta, \Delta\dot{\theta}, \Delta w\}$	6 $\{\Delta\psi, \Delta\theta, \Delta\varepsilon, \Delta M_{tfa}, \Delta\underline{M}_{bflap}\}$
③	R3 spd reg., per. ind. pitch	2 $\{\psi, \varepsilon\}$	9 $\{\Delta\underline{q}, \Delta\underline{\dot{q}}, \Delta\underline{\theta}, \Delta\underline{\dot{\theta}}, \Delta w\}$	4 $\{\Delta\psi, \Delta\underline{\theta}, \Delta\varepsilon\}$
④	R3, per. ind. pitch	7 $\{\tau_1, \tau_2, \psi, \varepsilon, \phi, \beta_1, \beta_1\}$	19 $\{\Delta\underline{q}, \Delta\underline{\dot{q}}, \Delta\underline{\theta}, \Delta\underline{\dot{\theta}}, \Delta w\}$	9 $\{\Delta\psi, \Delta\underline{\theta}, \Delta\varepsilon, \Delta\phi, \Delta M_{tfa}, \Delta M_{tss}, \Delta\underline{M}_{bflap}\}$
⑤	R2, TI coll. pitch	5 $\{\tau_1, \psi, \varepsilon, \beta_1, \beta_2\}$	14 $\{\Delta\underline{q}, \Delta\underline{\dot{q}}, \Delta\theta, \Delta\dot{\theta}, \int\Delta\theta, \Delta w\}$	7 $\{\Delta\psi, \Delta\theta, \Delta\varepsilon, \int\Delta\theta, \Delta M_{tfa}, \Delta\underline{M}_{bflap}\}$
⑥	R2 per. ind. pitch	5 $\{\tau_1, \psi, \varepsilon, \beta_1, \beta_2\}$	17 $\{\Delta\underline{q}, \Delta\underline{\dot{q}}, \Delta\underline{\theta}, \Delta\underline{\dot{\theta}}, \int\Delta\underline{\theta}, \Delta w\}$	9 $\{\Delta\psi, \Delta\underline{\theta}, \Delta\varepsilon, \int\Delta\underline{\theta}, \Delta M_{tfa}, \Delta\underline{M}_{bflap}\}$

Table 7: SymDyn measurement variables and the CART output channels used to calculate them

SymDyn Measurement(s)	CART Output Channel Number(s)	Description	Units
ψ	16	High-speed shaft position corrected for discontinuities, in the rotor reference frame	rad
$\underline{\theta}$	6, 8	Blade pitch angles	rad
$\int\Delta\underline{\theta}$	-	Numerical integral of $\Delta\underline{\theta}$	rad.s
ε	10	Low-speed shaft torque divided by modeled drive-train stiffness (26900 kNm/rad)	rad
ϕ	4	Hub teeter angle	rad
$\underline{M}_{bflap}$	12, 14	Blade root flap bending moments	Nm
M_{tfa}, M_{tss}	17, 46, 47	Tower bending moments decomposed into fore-aft and side-to-side directions using yaw error	Nm

6.2 ADAMS Simulation Results

Testing the control designs with an ADAMS simulation model is one of the last steps before field implementation. ADAMS results provide us with our most accurate performance measures because the model includes the effect of unmodeled higher-order structural dynamics. Below, brief comparisons are made of the most complex control algorithms that were field-tested (test cases 2, 4, 5, and 6 from

Table **6**) against the baseline controller. In each case, a 100-second turbulent wind file is used with dynamic stall and generalized dynamic wake options activated in AeroDyn.

In Region 3, the state-space pitch controllers are designed to have approximately the same RMS speed error as the baseline PI design but with improved fatigue performance. The results in Table 8 clearly show that both the time-invariant collective pitch design and the periodic individual pitch design offer these advantages.

Table 8: ADAMS simulation results for Region 3 controllers

Performance Measure	Baseline Controller	TI Coll. Pitch (Test Case 2)	Per. Ind. Pitch (Test Case 4)
RMS speed error (rpm)	0.389	0.380	0.369
Max. pitch rate (deg/s])	14.9	15.5	9.5
Max. pitch accel. (deg/s^2)	69	143	148
RMS pitch accel. (deg/s^2)	17	32	28
Tower fore-aft fatigue DEL (kNm)	2266	1586 (-30%)	1068 (-53%)
Tower side-to-side fatigue DEL (kNm)	285	n/a	103 (-64%)
Low-speed shaft fatigue DEL (kNm)	42	25 (-40%)	26 (-38%)
Blade-root flap fatigue DEL (kNm])	385	306 (-21%)	245 (-36%)

The Region 2 controller results are shown in Table 9. During all simulations, the tower resonance avoidance scheme described in Section 3 was not added, even for the baseline controller. It is clear from the results table that the state-space controllers, with their small pitch commands, do not adversely affect the power capture performance. However, the controllers are only effective in reducing the tower fore-aft fatigue damage and have little or no effect on the other fatigue measures. The lack of enhanced damping in the in-plane motions, i.e., tower side-to-side and shaft twist, can be explained by the fact that in Region 2 the turbine operates near the ridge of the torque coefficient curve. Therefore, pitch actions from a linear controller have little or no effect. Since tower side-to-side motion cannot be actively damped, the tower resonance avoidance scheme is still a necessary component of the algorithm.

Table 9: ADAMS simulation results for Region 2 controllers

Performance Measure	Baseline Controller	TI Coll. Pitch (Test Case 5)	Per. Ind. Pitch (Test Case 6)
Mean shaft power (kW)	187.85	187.54 (-0.17%)	187.59 (-0.14%)
Max. pitch rate (deg/s)	0	11.3	12.0
Max. pitch accel. (deg/s^2)	0	65	86
RMS pitch accel. (deg/s^2)	0	16	16
Tower fore-aft fatigue DEL (kNm)	1366	595 (-56%)	682 (-50%)
Tower side-to-side fatigue DEL (kNm)	355	n/a	317 (-11%)
Low-speed shaft fatigue DEL (kNm)	38	36 (-5%)	37 (-3%)
Blade-root flap fatigue DEL (kNm)	277	283 (+2%)	279 (+1%)

6.3 CART Test Results

The performance of an implemented state-space controller in Region 2 is compared with that of the baseline controller by plotting tower bending moment power-spectral-densities (PSDs), as shown in Figure 10 and Figure 11. The baseline control data are from file 11182058.dat, collected on November 18, 2002. The rotor speed range over the entire 10-minute dataset is 19 to 34 rpm. The time-invariant collective pitch state-space controller (from test case 5) was tested on June 9, 2003, and CART output was recorded in file 06091324.dat. This dataset was chosen because, between 110 and 550 seconds in the set, the rotor speed range is 18 to 34 rpm, which is very similar to the baseline case.

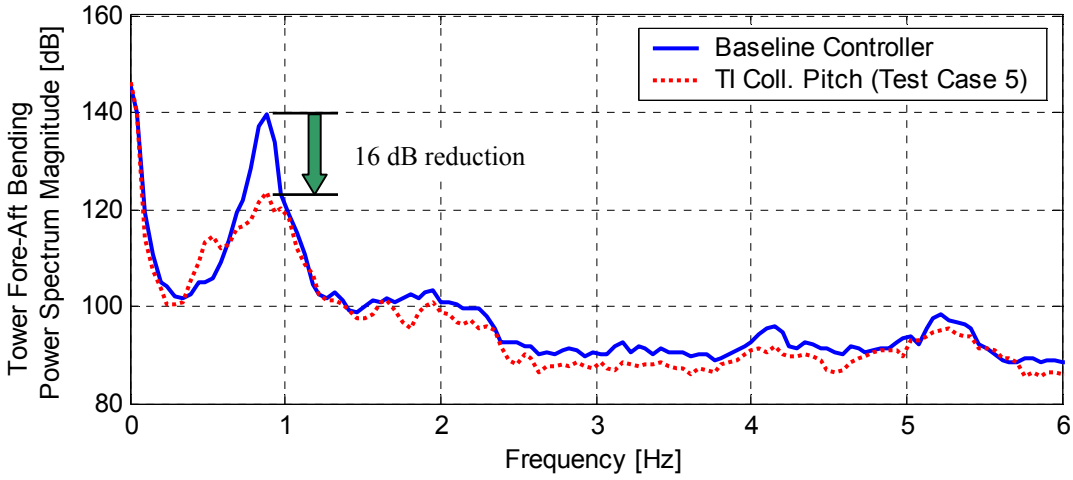

Figure 10: Tower fore-aft bending moment PSD plot for controller comparison in Region 2

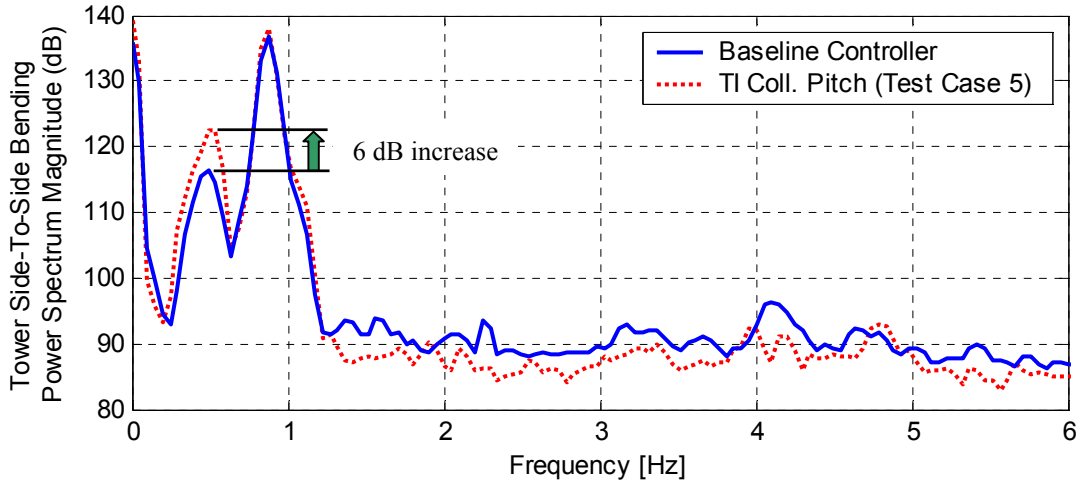

Figure 11: Tower side-to-side bending moment PSD plot for controller comparison in Region 2

The tower fore-aft bending moment PSD (Figure 10) illustrates the effectiveness of the state-space pitch controller to enhance damping in the first tower bending mode at approximately 0.9 Hz. While the baseline controller includes the tower resonance avoidance scheme (to keep rotor speeds away from 26 rpm), the state-space control data analyzed does not – the scheme was not introduced until a later date. Since the state-space controller does not enhance damping to tower side-to-side motion, it is likely that the use of the resonance avoidance scheme by the baseline controller would explain why this algorithm has a lower bending moment power spectrum magnitude (Figure 11) at approximately 0.5 Hz.

Figure 12 shows the collective pitch response from the state-space controller over 50 seconds of the dataset. As required, the controller makes very small adjustments to pitch angle to enhance damping without moving far from the optimal pitch of -1.0 deg and sacrificing energy capture.

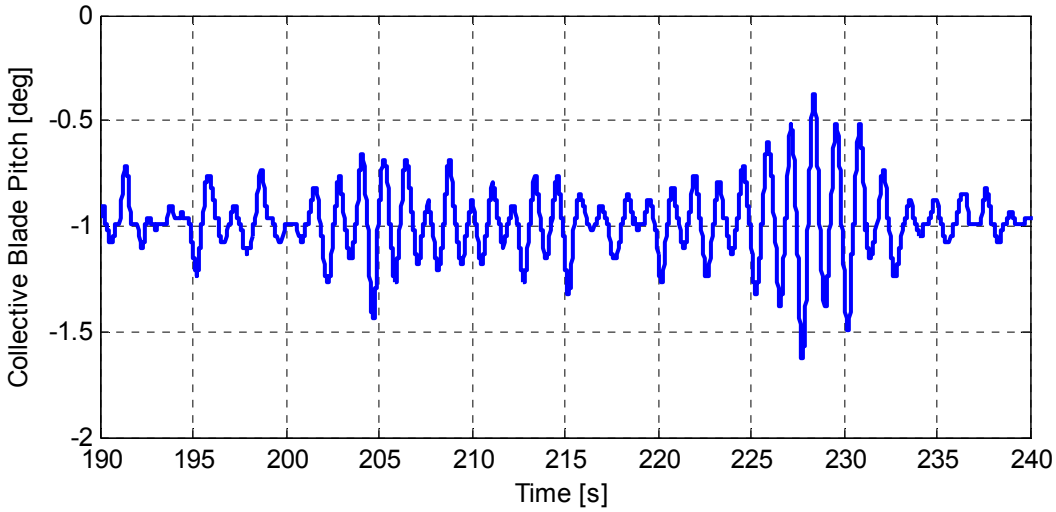

Figure 12: Collective blade pitch response for a time-invariant state-space controller in Region 2 (from 06091324.dat)

7. RECOMMENDATIONS FOR FUTURE WORK

- Improve the Region Transition Algorithm

  The adopted method of region transition, using the value of 95% of the rated rotor speed to switch between Region 2 and 3 control designs, could be much improved. Instead of saturating pitch angle to -1.0 deg when operating in Region 3, the Region 2 controller could become active. This would require other variables besides rotor speed to determine when to switch between regions, with some form of hysteresis.

- Enhance Tower Side-to-Side and Drive Train Damping in Region 2

  Using linear control and pitch alone to dampen in-plane vibration modes has not been successful in Region 2. The nonlinear aerodynamics prevent pitch actions from having the desired effect. One approach to solving this problem would be to use generator torque as the actuation method. In this case, blade pitch could still be employed to reduce tower fore-aft motion.

- Collect Additional Data for Statistical Performance Comparisons

  Insufficient data have been collected to allow a meaningful performance assessment of the state-space controller designs. Comparisons with the baseline data should be made statistically to ensure matching of wind and atmospheric conditions.

- Resolve Problems in Test Case 6

  Because of a lack of time, the control designs in test case 6 (periodic control in Region 2) have not been adequately tested. One problem is the observed high pitch rates that were not present in the SymDyn or ADAMS simulations.

8. ACKNOWLEDGEMENTS

The authors wish to thank Alan Wright and Katie Johnson at the National Wind Technology Center for their fruitful control discussions and help with all things CART. This report is supported under subcontract AAM-3-33231-01 with the National Renewable Energy Laboratory.

9. REFERENCES

[1] Bossanyi, E.A., 2003, "Individual Blade Pitch Control for Load Reduction," *J. Wind Energy*, **6**, pp. 119-128.

[2] Liebst, B.S., 1983, "Pitch Control for Large-Scale Wind Turbines," *J. Energy*, **7**, pp. 182-192.

[3] Mattson, S.E., 1984, "Modeling and Control of Large Horizontal Axis Wind Power Plants," Ph.D. thesis, Lund Institute of Technology, Lund, Sweden.

[4] Wright, A.D., 2003, "Modern Control Design for Flexible Wind Turbines," Ph.D. thesis, University of Colorado at Boulder, Boulder, CO.

[5] Stol, K.A., 2001, "Dynamics Modeling and Periodic Control of Horizontal-Axis Wind Turbines," Ph.D. thesis, University of Colorado at Boulder, Boulder, CO.

[6] Stol, K.A., 2003, "Disturbance Tracking and Blade Load Control of Wind Turbines in Variable-Speed Operation," *Proc. 22nd ASME Wind Energy Symposium*, Reno, Nevada, pp. 317-323.

[7] Fingersh, L.J., and Johnson, K.E., 2002, "Controls Advanced Research Turbine (CART) Commissioning and Baseline Data Collection," NREL/TP-500-32879, National Renewable Energy Laboratory, Golden, CO.

[8] Fingersh, L.J., and Johnson, K.E., 2004, "Baseline Results and Future Plans for the NREL Controls Advanced Research Turbine," *Proc. 23rd ASME Wind Energy Symposium*, Reno, Nevada.

[9] Stol, K.A., 2003, "Geometry and Structural Properties for the Controls Advanced Research Turbine (CART) from Model Tuning," NREL/TP-500-32087, National Renewable Energy Laboratory, Golden, CO.

[10] Stol, K.A., and Bir, G.S., 2003, "User's Guide for SymDyn, Version 1.2," NREL/EL-500-33845, http*://wind.nrel.gov/designcodes/symdyn/ symdyn.pdf*, accessed July 31, 2003, National Renewable Energy Laboratory, Golden, CO.

[11] Laino, D.J., and Hansen, A.C., 2002, "User's Guide to the Wind Turbine Aerodynamics Computer Software AeroDyn," Version 12.50, *http://wind.nrel.gov/designcodes/aerodyn/aerodyn.pdf*, accessed December 24, 2002.

[12] Kwakernaak, H., and Sivan, R., 1972, *Linear Optimal Control Systems*, Wiley Interscience, NY.

[13] Johnson, C.D., 1976, "Theory of Disturbance Accommodating Controllers," *Advances in Control and Dynamic Systems*, **12**, ed. C.T. Leondes.

[14] Downing, S.D. and Socie, D.F., 1982, "Simple Rainflow Counting Algorithms," *International Journal of Fatigue*, **4-1**, pp. 31-34.

[15] Miner, A.A., 1945, "Cumulative Damage in Fatigue," *Trans. ASME*, **67**, p. A159.

APPENDIX A: CART PITCH ACTUATOR MODEL

To obtain the pitch rate actuator model described in Section 2.1, field test data were analyzed. On 31 January 2003, preliminary state-space control algorithms were run on the CART. During the 10-minute data file 01311725.dat collected on that day, the turbine operated in Region 3, and pitch rate commands were sent to the electromechanical pitch actuators. Region 3 occurred between 240 seconds and 430 seconds into the data file, which was identified by low-speed shaft speeds being greater than 41 rpm and measured pitch angles being greater than -1 degree.

Given an assumed first-order form for the pitch rate, given by

$$\frac{\dot{\theta}(s)}{\dot{\theta}_{com}(s)} = \frac{K}{s+K}, \tag{A1}$$

the model pole K was found by solving the following minimization problem:

$$\min_{K} \text{norm}\left(\dot{\theta}_{meas}(t) - \dot{\theta}(t)\right), \tag{A2}$$

where $\dot{\theta}_{meas}(t)$ is the measured pitch rate response and $\dot{\theta}(t)$ is the solution of (A1). This problem is equivalent to least-squares fitting of pitch rate data.

The solution of (A2) over the 190 seconds of data analyzed is K = 60. Figure A.1 illustrates the fit between the actuator model response (dashed line) and the measured data (dotted line). It is obvious from the high-frequency variation in the measured signal that higher-order dynamic effects, such as blade torsional stiffness and aerodynamic pitch moments, are neglected by the first-order approximation.

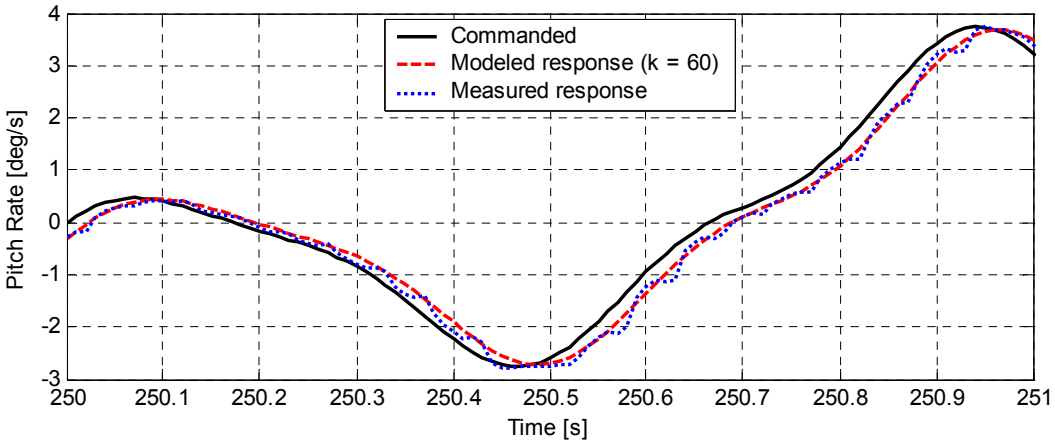

Figure A.1: Comparison of pitch rate signals over 1.0 second (from 01311725.dat)

APPENDIX B: INDEX OF TEST CASES AND DATA COLLECTED

Six tables are presented, corresponding to the six test cases of state-space control that were implemented on the CART between 1/2/03 and 8/4/03. Each table has seven columns, described below.

Column 1: **SymDyn DOFs**

Number of SymDyn degrees of freedom (DOFs) in the control model followed by an ordered list of these DOFs.

Column 2: **Number of States**

Number of states in the controller. The states are $\{\Delta\underline{q}, \Delta\dot{\underline{q}}, \Delta\underline{\theta}, \Delta\dot{\underline{\theta}}, \Delta w\}$ unless otherwise listed (where $\underline{q}$ are the SymDyn DOFs). Note that for the collective pitch controllers, $\Delta\underline{\theta}$ and $\Delta\dot{\underline{\theta}}$ contain only one state each.

Column 3: **Measurements**

Number of CART measurements used by the controller followed by an ordered list of these measurements.

Column 4: **LQR Weightings**

Matrix weightings for the full-state feedback design (Q, R) and state estimator design (Q^E, R^E). The diagonal entries of each matrix are listed.

Column 5: **Gain Set #**

Gain set reference number for the control design. The reference number also appears in the first line of the control array input file (ctrlarr.dat, ctrlarr2.dat, or ctrlarr3.dat). When a controller is used in conjunction with another controller (where one is for Region 2 and the other for Region 3), the complementary gain set number is listed, e.g., 14 (w/15).

Column 6: **Test Data**

List of 10-minute test data files collected. Only the first and last data files in a consecutive set are listed, separated by a hyphen. The '.dat' file extension of each file is omitted for brevity. Data files may be appear in two tables when both Region 2 and Region 3 controller designs are used to collect the data.

Column 7: **Code Changes and Comments**

Notes describing the changes made to the computer code and comments (in italics) describing the performance of the control algorithm.

Listed at the bottom of each table is the total number of hours of data collected for the corresponding test case.

① Speed regulation in Region 3 using LTI collective pitch

SymDyn DOFs	Number of States	Measurements	LQR Weightings	Gain Set #	Test Data	Code Changes and *Comments*
1 $\{\psi\}$	3 $\{\Delta q, \Delta\dot{q}, \Delta w\}$	1 $\{\Delta\psi_{LSS}\}$ [1]	$Q = [0, 0.5]$, $R = 1$ $Q^E = [10^2, 10^5, 10^7]$, $R^E = 1$	1	01021803, 01131744- 01131754	*Drive train excited.*
			$Q = [0, 0.5]$, $R = 1$ $Q^E = [10^2, 10^5, 10^8]$, $R^E = 1$	2	never tested	
			$Q = [0, 10]$, $R = 1$ $Q^E = [10^2, 10^5, 10^7]$, $R^E = 1$	3	never tested	
4 $\{\psi, \varepsilon, \beta_1, \beta_2\}$	9 $\{\Delta q, \Delta\dot{q}, \Delta w\}$	1 $\{\Delta\psi_{LSS}\}$	$Q = [0,0,0,0, 2,0,1,1]$, $R = 1$ $Q^E = [10^2,0,0,0, 10^5,0,0,0, 10^7]$, $R^E = 1$	4	01151903, 01151920	*Drive train excited.*
1 $\{\psi\}$	5	2 $\{\Delta\psi, \Delta\theta\}$ [2]	$Q = [5,40, 0,0]$, $R = 1$ $Q^E = [1,10^3, 1,1, 10^5]$, $R^E = [1,1]$	5	01311725, 01311736	Pitch actuator dynamics added to controller and azimuth error now measured using HSS position. *Speed overshoot due to windup.*
				6	02102047, 02111657, 02111712	Bug fixed. Added fixed azimuth error saturation at –20º. *Pitch jumps during saturation.*
				6	02202032- 02202112, 02210113- 02210123	Automatic azimuth error saturation added. *Speed overshoot due to windup.*
				6	03052151- 03052211, 03052226- 03052306, 03061752- 03061812, 03061826- 03061836, 03062008- 03062038	Returned to manual azimuth error saturation with better logic. *Good performance.*
					5.7 hours	

[1] The measurement signal $\Delta\psi_{LSS}$ is the generator azimuth error (in low-speed-shaft frame) measured using the low-speed-shaft position signal.

[2] $\Delta\psi$ is measured using the high-speed-shaft position signal for better resolution.

② Fatigue mitigation in Region 3 using LTI collective pitch

SymDyn DOFs	Number of States	Measurements	LQR Weightings	Gain Set #	Test Data	Code Changes and *Comments*
5 $\{\tau_1, \psi, \varepsilon, \beta_1, \beta_2\}$	13	2 $\{\Delta\psi, \Delta\theta\}$	$Q = [0,2,0,0,0, 0,2,0,0,0, 0,0]$, $R = 1$ $Q^E = [1,1,1,1,1, 1,1,1,1,1, 1,1, 10^{10}]$, $R^E = [1,1]$	7	03122307	*Appears unstable in simulator at tower frequency.*
				7	03150258	Bug fixed. *Drive train excited.*
				7	04152153- 04152213	Different azimuth error saturation method. *Drive train and tower fore-aft excited.*
			$Q = [0,5,0,0,0, 0,40,0,0,0, 0,0]$, $R = 1$ $Q^E = [1,1,1,1,1, 1,10^3,1,1,1, 1,1, 10^8]$, $R^E = [1,1]$	8	04042159- 04042209	*Drive train excited due to poor gains.*
		3 $\{\Delta\psi, \Delta\theta, \Delta\varepsilon\}$	$Q = [0,10,0,10^3,10^3, 10^2,20,0,0,0, 0,0]$, $R = 1$ $Q^E = [1,1,10^5,1,1, 1,10^3,1,1,1, 1,1, 10^{10}]$, $R^E = [1,1,1]$	9	04161908, 04181700- 04181720	*No drive train or tower excitation. Speed regulation could be improved.*
			$Q = [0,20,0,10^3,10^3, 10^3,40,0,0,0, 0,0]$, $R = 1$ $Q^E = [1,1,10^5,1,1, 1,10^3,1,1,1, 1,1, 10^{10}]$, $R^E = [1,1,1]$	10	04181738, 04181825- 04182025, 04182207- 04182237, 04182259	*Good performance. Large amounts of Region 3 data.*
		6 $\{\Delta\psi, \Delta\theta, \Delta\varepsilon,$ $\Delta M_{tfa}, \Delta \underline{M}_{bflap}\}$	$Q = [0,5,0,500,500, 500,40,0,0,0, 0,0]$, $R = 1$ $Q^E = [1,1,10^2,10^2,10^2, 1,10^5,1,1,1, 1,1, 10^5]$, $R^E = [1,1,1,1,10^{15},10^{13},10^{13}]$	14 (w/15)	05212032, 05212053, 05302029	Added state-space control in Region 2. *See Region 2 notes.*
				14 (w/16)	05272251, 05281340- 05281400, 05291431- 05291441, 05292232, 05300101- 05300111, 05300133	*See Region 2 notes.*
				14 (w/17)	06030429, 06041756- 06041816, 06051401, 06091324	*See Region 2 notes.*

				14 (w/17)	06102258-06102328	Added state estimate handoff between regions. *Overspeed.*
				14 (w/17)	06201911	Fixed region transition bug. *Overspeed.*
			$Q = [0,20,0,500,500,\ 500,40,0,0,0,\ 0,0]$, $R = 1$ $Q^E = [1,1,10^2,10^2,10^2,\ 1,10^5,1,1,1,\ 1,1,\ 10^5]$, $R^E = [1,1,1,10^{15},10^{13},10^{13}]$	18 (w/17)	06290556-06290626, 07152125, 07161348-07161438, 07162135-07162205, 07212058-07220008, 07241327-07241427	*Good performance. See region 2 notes.*
					07281346-07281526	*See region 2 notes.*
				18 (w/17)	07291958	Minor bug fixed. *Blade1 flap moment signal error (water under strain gauge) causes high dynamic loads and slip-ring failure.*
					18.0 hours	

③ Speed regulation in Region 3 using periodic IBC

SymDyn DOFs	Number of States	Measurements	LQR Weightings	Gain Set #	Test Data	Code Changes and *Comments*
2 $\{\psi, \varepsilon\}$	9	4 $\{\Delta\psi, \Delta\underline{\theta}, \Delta\varepsilon\}$	$Q = [5,0,\ 10,0,\ 0,0,0,0]$, $R = [1,1]$ $Q^E = [1,1,\ 1,1,\ 1,1,1,1,\ 10^7]$, $R^E = 1$	11	04231847-04231857, 04232010	*Poor speed regulation. Drive train excited.*
					0.5 hours	

④ Fatigue mitigation in Region 3 using periodic IBC

SymDyn DOFs	Number of States	Measurements	LQR Weightings	Gain Set #	Test Data	Code Changes and *Comments*
6 $\{\tau_1, \psi, \varepsilon, \phi, \beta_1, \beta_2\}$	17	7 $\{\Delta\psi, \Delta\underline{\theta}, \Delta\varepsilon, \Delta\phi, \Delta\underline{M}_{\text{bflap}}\}$	$Q = [0,1,0,5,10^2,10^2, 0,30,0,0,0,0, 0,0,0,0]$, $R = [1,1]$ $Q^E = [1,1,1,10^2,10^2,10^2, 1,10^5,1,1,1,1, 1,1,1,1, 10^5]$, $R^E = [1,1,1,1,1,10^{13},10^{13}]$	12	05051738- 05051748	*Poor speed regulation.*
			$Q = [0,1,0,5,10^2,10^2, 0,30,0,0,0,0, 0,0,0,0]$, $R = [1,1]$ $Q^E = [1,1,10^2,10^2,10^2,10^2, 1,10^5,1,1,1,1, 1,1,1,1, 10^5]$, $R^E = [1,1,1,1,1,10^{13},10^{13}]$	13	05132141- 05132221, 05190226- 05190236	Different azimuth error saturation method. *Good performance.*
7 $\{\tau_1, \tau_2, \psi, \varepsilon, \phi, \beta_1, \beta_1\}$	19	9 $\{\Delta\psi, \Delta\underline{\theta}, \Delta\varepsilon, \Delta\phi,$ $\Delta M_{\text{tfa}}, \Delta M_{\text{tss}}, \Delta\underline{M}_{\text{bflap}}\}$	$Q = [0,0,10,0,10^2,10^3,10^3, 10^3,10^4,40,0,0,0,0, 0,0,0,0]$, $R = [1,1]$ $Q^E = [1,1,1,1,1,1,1,1, 10^3,10^2,10^5,10^5,10^5,10^5,10^5, 1,1,1,1, 10^6]$, $R^E = [1,1,1,1,1,10^{15},10^{15},10^{13},10^{13}]$	20 (w/19)	08042020- 08042050	Added state-space control in Region 2. *Region 2 data only.*
					2.2 hours	

⑤ Fatigue mitigation in Region 2 using LTI collective pitch

SymDyn DOFs	Number of States	Measurements	LQR Weightings	Gain Set #	Test Data	Code Changes and *Comments*
5 $\{\tau_1, \psi, \varepsilon, \beta_1, \beta_1\}$	13	6 $\{\Delta\psi, \Delta\theta, \Delta\varepsilon, \Delta M_{\text{tfa}},$ $\Delta\underline{M}_{\text{bflap}}\}$	$Q = [0,0,0,10^4,10^4, 10^5,0,0,0,0, 10^4,0]$, $R = 1$ $Q^E = [1,1,10^2,10^2,10^2, 1,10^5,1,1,1, 1,1, 10^5]$, $R^E = [1,1,1,10^{15},10^{13},10^{13}]$	15 (w/14)	05212032, 05212053	*Pitch not centered on –1° and no apparent reduction in tower motion.*
			$Q = [0,0,0,0,0, 10^4,0,0,0,0, 10^4,0]$, $R = 1$ $Q^E = [1,1,10^2,10^2,10^2, 1,10^5,1,1,1, 1,1, 10^5]$, $R^E = [1,1,1,10^{15},10^{13},10^{13}]$	16 (w/14)	05272251, 05281340- 05281400, 05291431- 05291441, 05292232, 05300101- 05300111, 05300133	Integer overflow bug fixed. *Same problems.*

				15 (w/14)	05302029	Returned to earlier gain set. Tower signal bug fixed. *Good tower fore-aft damping but pitch not centered on –1°.*
5 $\{\tau_1, \psi, \varepsilon, \beta_1, \beta_1\}$	14 $\{\Delta\underline{q}, \Delta\dot{\underline{q}}, \Delta\theta, \Delta\dot{\theta}, \int\Delta\theta, \Delta w\}$	7 $\{\Delta\psi, \Delta\theta, \Delta\varepsilon, \int\Delta\theta, \Delta M_{tfa}, \Delta\underline{M}_{bflap}\}$	$Q = [0,0,0,0,0, 10^4,0,0,0,0, 0,0,10^3]$, $R = 1$ $Q^E = [1,1,10^2,10^2,10^2, 1,10^5,1,1,1, 1,1,1, 10^5]$, $R^E = [1,1,1,1,10^{15},10^{13},10^{13}]$	17 (w/14)	06030429, 06041756-06041816, 06051401, 06091324	*Good tower fore-aft damping and pitch centering. Tower side-to-side excited.*
				17 (w/14)	06102258-06102328	Added state estimate handoff between regions. *Overspeed.*
				17 (w/14)	06201911	Fixed region transition bug. *Overspeed.*
				17 (w/18)	06290556-06290626, 07152125, 07161348-07161438, 07162135-07162205, 07212058-07220008, 07241327-07241427	Added original tower resonance avoidance scheme since side-to-side motion is not damped. *Good performance.*
					07281346-07281526	*Low region 2 data. Speed sticking at controller start*
				17 (w/18)	07291958	Minor bug fixed. *See Region 3 notes.*
					13.0 hours	

⑥ Fatigue mitigation in Region 2 using periodic IBC

SymDyn DOFs	Number of States	Measurements	LQR Weightings	Gain Set #	Test Data	Code Changes and *Comments*
5 $\{\tau_1, \psi, \varepsilon, \beta_1, \beta_1\}$	17 $\{\Delta\underline{q}, \Delta\dot{\underline{q}}, \Delta\underline{\theta}, \Delta\dot{\underline{\theta}}, \int\Delta\underline{\theta}, \Delta w\}$	9 $\{\Delta\psi, \Delta\underline{\theta}, \Delta\varepsilon, \int\Delta\underline{\theta}, \Delta M_{tfa}, \Delta\underline{M}_{bflap}\}$	$Q = [0,0,0,0,0, 10^4,0,0,0,0, 0,0,0,0,10^3,10^3]$, $R = [1,1]$ $Q^E = [1,1,10^2,10^2,10^2, 1,10^5,1,1,1, 1,1,1,1,1,1, 10^5]$, $R^E = [1,1,1,1,1,1, 10^{15},10^{13},10^{13}]$	19 (w/20)	08042020-08042050	*High pitch rates.*
					0.7 hours	

REPORT DOCUMENTATION PAGE

Form Approved
OMB No. 0704-0188

PLEASE DO NOT RETURN YOUR FORM TO THE ABOVE ORGANIZATION.

1. REPORT DATE *(DD-MM-YYYY)*	2. REPORT TYPE	3. DATES COVERED *(From - To)*
September 2004	Subcontract Report	August 25 - November 30, 2003

4. TITLE AND SUBTITLE
Wind Turbine Field Testing of State-Space Control Designs

5a. CONTRACT NUMBER
DE-AC36-99-GO10337

5b. GRANT NUMBER

5c. PROGRAM ELEMENT NUMBER

6. AUTHOR(S)
K.A. Stol (University of Auckland)
L.J. Fingersh (NREL)

5d. PROJECT NUMBER
NREL/SR-500-35061

5e. TASK NUMBER
WER4 3301

5f. WORK UNIT NUMBER

7. PERFORMING ORGANIZATION NAME(S) AND ADDRESS(ES)
The University of Auckland
Private Bag 92019
Auckland, New Zealand

8. PERFORMING ORGANIZATION REPORT NUMBER
AAM-3-33231-01

9. SPONSORING/MONITORING AGENCY NAME(S) AND ADDRESS(ES)
National Renewable Energy Laboratory
1617 Cole Blvd.
Golden, CO 80401-3393

10. SPONSOR/MONITOR'S ACRONYM(S)
NREL

11. SPONSORING/MONITORING AGENCY REPORT NUMBER
NREL/SR-500-35061

12. DISTRIBUTION AVAILABILITY STATEMENT
National Technical Information Service
U.S. Department of Commerce
5285 Port Royal Road
Springfield, VA 22161

13. SUPPLEMENTARY NOTES
NREL Technical Monitor: A. Wright

14. ABSTRACT *(Maximum 200 Words)*

This report investigates the application of advanced pitch control algorithms on a 600 kW variable-speed, variable-pitch wind turbine known as the Controls Advanced Research Turbine (CART). A design approach is outlined to test both time-invariant and periodic control methods for fatigue load reduction over all operating wind speeds. Practical implementation issues are identified and addressed. Test data and preliminary performance comparisons are presented to support the approach.

15. SUBJECT TERMS
wind turbine; Controls Advanced Research Turbine; pitch control; fatigue load;

16. SECURITY CLASSIFICATION OF:			17. LIMITATION OF ABSTRACT	18. NUMBER OF PAGES	19a. NAME OF RESPONSIBLE PERSON
a. REPORT	b. ABSTRACT	c. THIS PAGE			
Unclassified	Unclassified	Unclassified	UL		19b. TELEPONE NUMBER (*Include area code)*

Standard Form 298 (Rev. 8/98)
Prescribed by ANSI Std. Z39.18